
EFFECT OF ADDITION OF SOME ORGANIC AND INORGANIC COMPOUNDS ON THE PITTING CORROSION OF STAINLESS STEEL ELECTRODES

A. S. I. AHMED*, R. M. ABOU SHAHBA*, E. M. ATTIA*, IBRAHIME M. GHAYAD** AND W. A. M. HUSSEIN*

* *Chemistry Department, Faculty of Science (for Girls), Al-Azhar University, Nasr City, Cairo, Egypt*

***Central metallurgical research and development iastitute*

Abstract

The corrosion behavior of two stainless steel electrodes with different chemical compositions in different salt solutions of Cl^- ions (NaCl , FeCl_3 and HgCl_2) was studied. The corrosion behavior in 3.5% NaCl with and without different concentrations of two different triazole derivatives, 3-amino-1, 2, 4 triazole (AT) and 4-amino-5-mercapto-1, 2, 4 triazole (AMT) and $\text{Na}_2\text{S}_2\text{O}_3$ (50 to 200ppm.) was studied. Open circuit potential measurements, potentiodynamic cyclic anodic polarization (PCAP) and surface morphology techniques were used in this study.

Obtained results showed that NaCl is more aggressive comparing with FeCl_3 and HgCl_2 . As the concentration of sodium chloride increased, the (PCAP) curves indicated the presence of pitting or crevice corrosion breakdown potential which sustained the increase of anodic current density. The plots of pitting potential (E_{pit}), or protection potential (E_p) versus $\log [\text{Cl}^-]$ at 25°C , for the two stainless steel electrodes were linearly decreased with the increase of the logarithm of chloride concentration. Also the increase of scan rate increases the localized pitting corrosion. The additions of sodium thiosulphate to 3.5% NaCl enhance pitting corrosion as compared with that found in pure sodium chloride solution. On the contrary, increasing concentration of (AT) and (AMT) in NaCl solution was found to greatly enhance IE%. The adsorptive behavior of the investigated inhibitors on the steel surface followed Langmiur-type isotherm. These results indicate the suitability of the use of the investigated inhibitors. Electrode type (I) has a greater tendency for pitting than electrode type (II) due to the percentage of nickel in electrode type (I) is half that of electrode type (II).

Introduction

Stainless steels have excellent corrosion resistance, which is principally due to their high chromium content. Nickel in sufficient amounts also improves their ductility and formability by making it possible for the austenitic structure to be retained at room temperature. Molybdenum, when added to stainless steels, improves corrosion resistance in the presence of chloride ions, whereas aluminum improves high-temperature scaling resistance. Other elements added to improve particular characteristics include copper, titanium, silicon, niobium, nitrogen, sulphur and selenium^(1, 2)

The electrochemical behaviors of passive film of stainless steel under the condition of static state and ultrasonic cavitation in the HCl solution indicate that the passive film shows a multilayer structure distribution ⁽³⁾. The corrosion inhibition in HCl solutions was studied in different types of steels. Derivatives of diazole, triazole, quinolin, lactones; have been investigated for the corrosion of mild steel in HCl at different concentrations using weight loss measurements, potentiodynamic polarization and impedance spectroscopy methods (EIS). Generally, inhibition efficiency of the investigated compounds was found to depend on the concentration and the nature of the inhibitors ⁽⁴⁻⁷⁾.

Potentiodynamic polarization, (EIS) and weight loss studies were also carried out on the inhibition of carbon steel in hydrochloric acid solution by the aqueous extract of olive and bipyrazolic compounds ^(8,9). The bipyrazolic compounds act as mixed-type inhibitors while pyrazolic derivatives are cathodic-type inhibitors in HCl solutions ^(10, 11).

Pickling of oxidized 304 stainless steels in single or multiple electrolytes was investigated based on weight loss and corrosion potential measurements. A smooth surface finish was obtained after an extended pickling in HCl, but some external oxide scales remained ^(12, 13).

This work may throw some light on corrosion behavior of two types of electrodes with different chemical composition in different Cl⁻ solutions and to evaluate corrosion inhibition.

Experimental

Electrodes:

Two electrodes of molybdenum alloyed stainless steel of special grades have been tested. Typical values of their chemical compositions are given in Table (1).

Table (1): Chemical composition of the two types of electrodes

Samples	Amount of Elements (%)					
	Si	Cr	Mn	Fe	Ni	Mo
Electrode (I)	1.27	18.72	1.86	70.65	5.05	2.45
Electrode (II)	0.56	17.28	1.14	67.83	10.57	2.62

Pretreatment of samples:

Cylindrical electrodes with a working surface area of 0.68 cm² were used. Electrodes were enclosed in a holder which can be made in contact with the test

solution. The electrodes were ground with emery paper and polished with diamond paste (1 μ m); finally the samples were cleaned by bi-distilled water and ethyl alcohol, and quickly inserted in the cell.

Electrolytes:

Analytical grade reagents were used in all experiments with bi-distilled water. The used electrolytes were:

Different concentrations of inorganic salts solutions like NaCl, FeCl₃ and HgCl₂ (0.5 to 14.2%) and Na₂S₂O₃ (50 to 200ppm.). Different concentrations of different triazole derivatives, 3-amino-1, 2, 4 triazole (AT) and 4-amino-5-mercapto-1, 2, 4 triazole (AMT) in concentration range of (0.25 to 4%).

Techniques:

Open-Circuit Technique:

Open-circuit measurements were carried out in conventional glass cell of 150ml solution. Potential was measured with respect to an external saturated calomel electrode (SCE) interfaced to the test solution via a salt bridge.

The working electrode was immersed vertically in the test solution and the potential was recorded as a function of time till steady state values were established. The potential measurements were carried out at room temperature (25 \pm 2 $^{\circ}$ C), using electronic multimeter (Type Escord EDM-2116).

Potentiodynamic Cyclic Anodic Polarization:

Potentiodynamic cyclic anodic polarization (PCAP) were measured using Autolab GPES 30 (General Purpose Electronically System, Eco Chemie B.V., Utrecht, The Netherlands). After attaining a steady rest potential ($E_{corr.}$), the electrode scanned at a rate of 1 mV/sec. Potential scan reversal was commenced at an applied current density of approximately 0.3 mA/cm².

Surface Morphology:

Once the cyclic anodic polarization curve is obtained the breakdown potential $E_{pit.}$, and the protection potential E_p . were deduced. The working electrode is then held at such a potential for at least one hour to enhance pitting corrosion, then the electrode removed from the holder, cleaned, dried and investigated under a metallurgical light microscope model (ASTM G46 Olympus Tokyo) to determine

shape, size and pit depth. In determining the pit depth, the microscope is focused on the lip of the pit, then on its bottom. The difference between the initial and final readings on the fine focusing knob of the microscope is the pit depth. The morphological micrographs were exposed at magnifications favored the purposes of investigation.

Results And Discussion

I- Open circuit potential measurements:

The effect of chloride ion concentration on the open-circuit potential values using different chloride media are shown in figures (1, 2). The concentrations of the chloride solutions were, 3.5% NaCl, 5.4% FeCl₃ and 14.2% HgCl₂, containing the same chloride ion percent.

Accordingly, the behavior can be classified into two different behaviors depending upon the type of the electrode. The first behavior which represented by the potential-time curves of electrode type (I) in all chloride test solutions, figure (1), these curves exhibit a dissolution or segregation of alloying elements in a solution and shooting of the potential to more positive values, being higher in FeCl₃ and NaCl, indicating the film formation and then the potential drops to more negative value until the steady state potential is reached. The results in HgCl₂ solution indicated that the potential shifted from positive to the negative direction with time until steady state potential is attained. The behaviors of all chloride solutions indicate the dissolution and corrosion.

The second behavior, on the other hand, belongs to the stainless steel electrode type (II) in all test solutions is recorded in figure (2). Inspection of these curves there is a general tendency for the open-circuit potential to shift from positive to more negative values than the initial potential, denoting the destruction of the pre-immersion oxide film present on the surface of the electrode.

Most chloride test solutions promote corrosion of the two electrodes and the extent of corrosion acceleration seems to depend on the nature of the test solution. It is suggested that the order runs as follows:



However, when stainless steels are exposed to environments containing certain aggressive anions such as the chloride ion, the stability of the passive state is impaired, and two localized forms of corrosion, known as pitting and crevice corrosion can occur. The exact mechanism of this impairment or breakdown process

is not known with certainty but is believed by many workers ⁽¹⁴⁾ to consist of a potential –controlled adsorption reaction involving chloride ions and specific sites on the metal surface. More specifically, when the condition of exposure are such that a certain potential drop occurs across the metal/solution interface, it has been proposed that the chloride ion displaces the passivating species at some locations

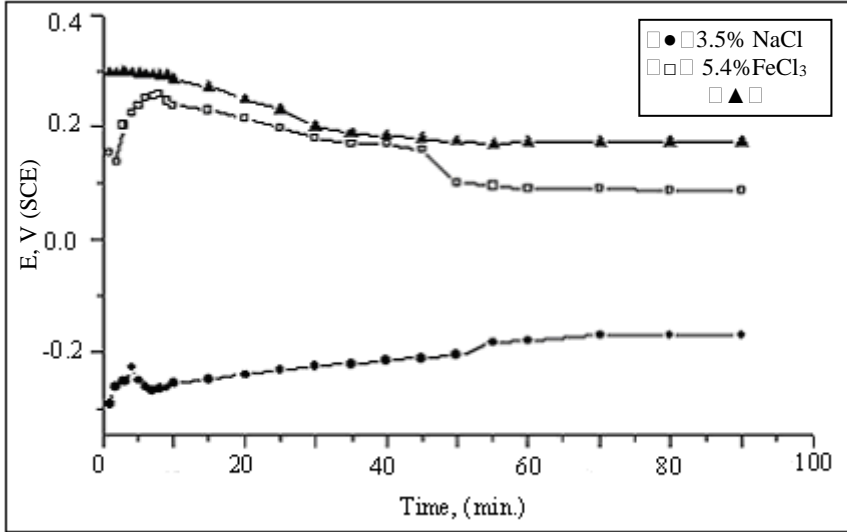


Figure (1): Potential– time curves of electrode (I) in different Cl⁻ solutions.

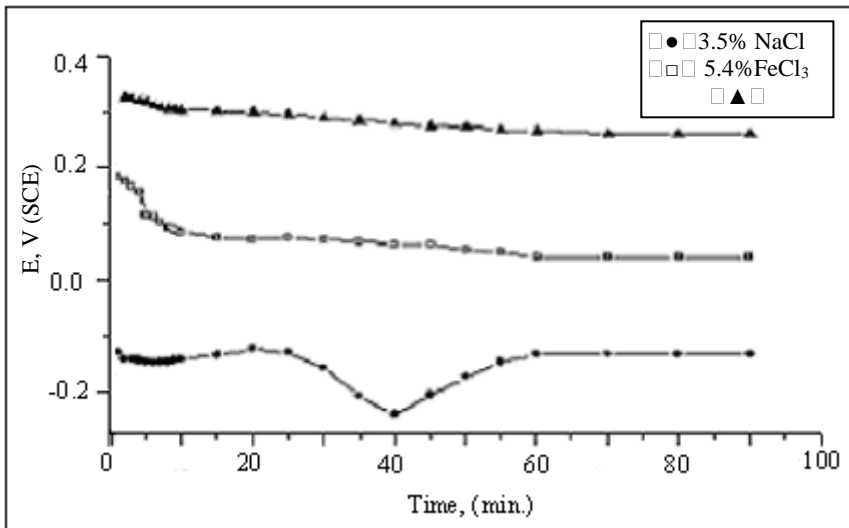
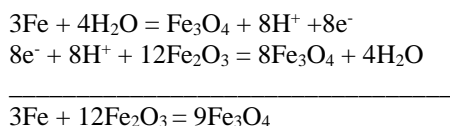


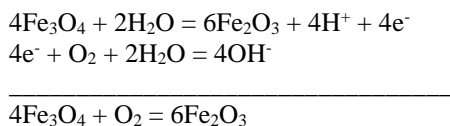
Figure (2): Potential– time curves of electrode (II) in different Cl⁻ solutions.

and promotes local rapid anodic dissolution (presumably by either lowering the dissolution over voltage or by initiating a different dissolution mechanism), thereby resulting in a pit nucleus.

The general shift of open-circuit potential to more active values indicates the attack of the base metal through the pores present in the oxide which is represented by the following equations⁽¹⁵⁾:



The general shift to noble direction points toward oxidation of Fe_3O_4 to Fe_2O_3 ,



The high positive shift indicates the high amount of Fe_2O_3 present in the oxide layer.

II- Potentiodynamic cyclic anodic polarization measurements:

A) Influence of chloride ions on the pitting corrosion of the two stainless steel electrodes using different chloride media:

As it is clear from figures 3 and 4 and Table (2) the applied potential scans beginning at E_{corr} and continuing in the positive (anodic) direction until a large increase in current occurs. When the scan reaches a certain current value, it reverses and begins scanning in cathodic direction. Generally, the reverse scans at a higher current level than the forward scan. The size of the pitting loop served as indication for pitting tendency; the larger the loop, the greater the tendency to pit.

It can be seen that the hysteresis loop is wide in NaCl solution and its size diminished in both FeCl_3 and HgCl_2 . These results indicated that, NaCl is more aggressive than FeCl_3 and HgCl_2 and that electrode type (I) has a greater tendency for pitting than electrode type (II) due to the percentage of nickel in electrode type (I) is half of electrode type (II). The results confirm that, the corrosion potential of

stainless steels is dependent on the cation type. It is well accepted that pitting of stainless steels is affected in two steps: one initiating step and one propagating step.

Most of the proposed mechanisms involve either an activating ion such as chloride, penetrating and destroying the passive film locally, or the activating ion being adsorbed at the metal/solution interface displacing the adsorbed passive layer and thus destroying the passivity locally. The potential setup between the locally disrupted film and the rest of the surface leads to anode formation and attack of the metal at some points. In both mechanisms the adsorption of the anion is important. The composition of the oxide film on the metal surface, which depends sensitively on the production of steel, must also have a great influence on the adsorption⁽¹⁶⁾.

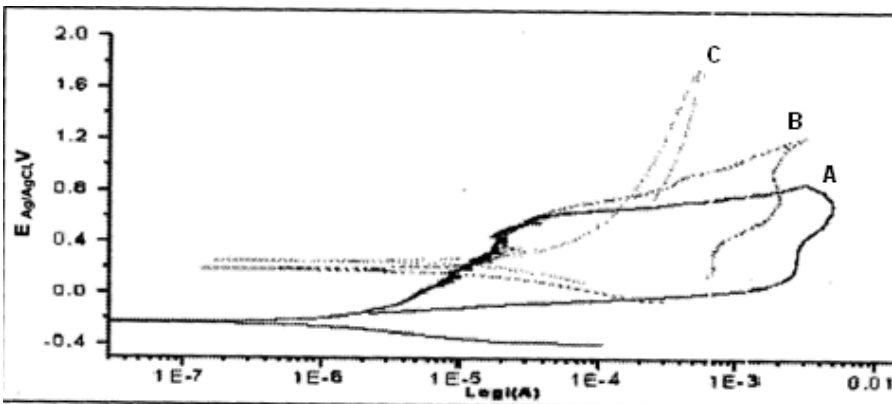


Figure (3) Cyclic anodic polarization curves of electrode type (I) in (A) 3.5% NaCl, (B) 5.39% FeCl₂ and (C) 14.126% HgCl₂ solutions.

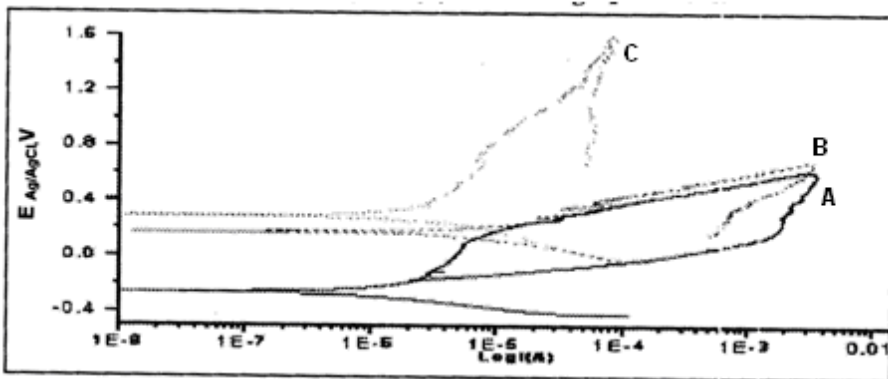


Figure (4) Cyclic anodic polarization curves of electrode type (II) in (A) 3.5% NaCl, (B) 5.39% FeCl₂ and (C) 14.126% HgCl₂ solutions.

Table (2): The corrosion parameters of electrodes (I) and (II) in different chloride solutions.

Medium	$E_{corr.}, V$		E_p, V		$E_{pit.}, V$	
	(I)	(II)	(I)	(II)	(I)	(II)
3.5% NaCl	-0.231	-0.259	-0.145	-0.163	0.456	0.227
5.4% FeCl ₃	0.179	0.172	0.179	0.166	--	0.356
14.2% HgCl ₂	0.242	0.284	--	--	--	--

B) Stainless steel electrodes in sodium chloride solutions:

Figures (5,6) represent the potentiodynamic cyclic anodic polarization (PCAP) measurements for stainless steel type (I) and (II) in different concentrations of sodium chloride solutions ranging from 0.5 to 5.5%, using scan rate 1mV/sec., in the potential range from -600 to 1500 mV_{Ag/AgCl} at 25°C.

It is clear that the polarization curves have the same general features and characterized by the appearance of active, passive and transpassive regions before oxygen evolution. After the corrosion potential, the anodic current density starts to increase to form the active region at low concentrations. The increase of the potential in the positive direction leads to increasing of the anodic current, which corresponds to the oxidation of iron to iron ions. With increasing the potential, a passive film [Fe(OH)₂, Fe₃O₄ and/or Fe₂O₃] can be formed⁽¹⁷⁾. When the potential moves towards more anodic, the current density starts to increase again, forming the transpassive region before oxygen evolution. The current is raised suddenly without any sign of oxygen evolution, at higher concentrations, denoting breakdown of the passive layer, when the polarization potential reaches a certain critical potential ($E_{pit.}$).

The results obtained from figures (5, 6) show that at a low concentration of sodium chloride (0.5%), there is a broad passive region with a passive current density of 8.1×10^{-5} and 1.419×10^{-5} A/cm² for electrodes (I) and (II), respectively. It is also observed that there is no sign for localized corrosion breakdown, until oxygen evolution takes place with little hysteresis loop on the reverse anodic scan which is attributed to the dissolution in the transpassive region^(15, 18).

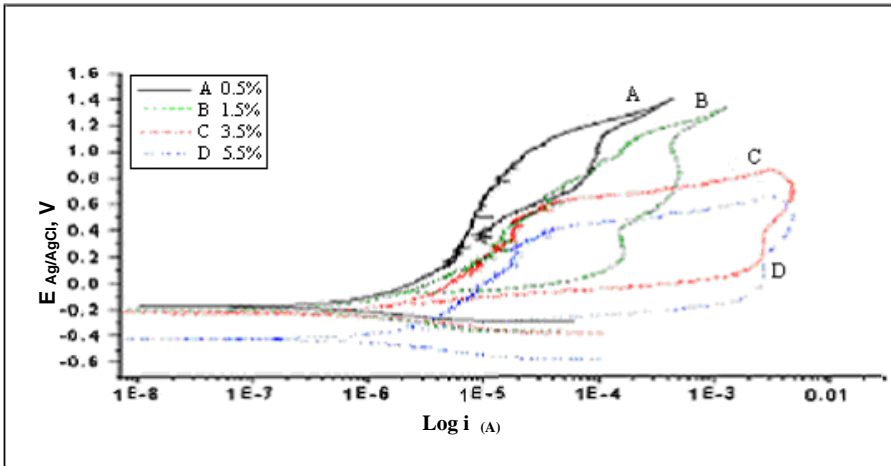


Figure (5): Cyclic anodic polarization curves of electrode (I) in (0.5-5.5%) NaCl solutions.

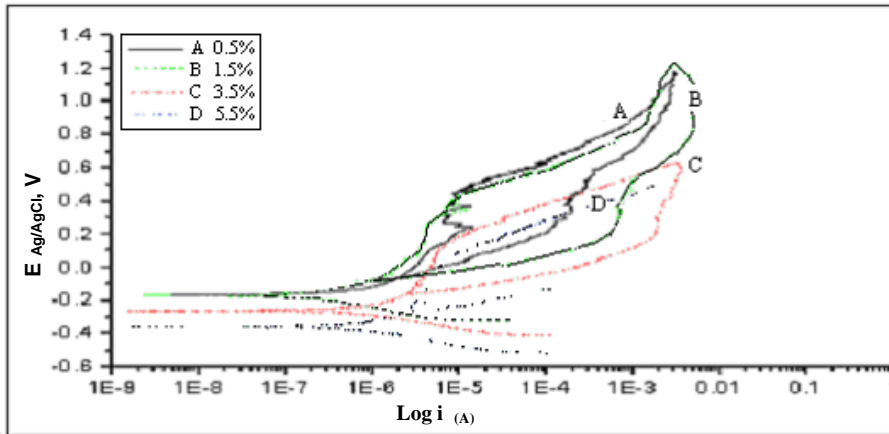


Figure (6): Cyclic anodic polarization curves of electrode type (II) in (0.5-5.5%) NaCl solutions.

As the concentration of sodium chloride increased the PCAP curves indicated the presence of pitting or crevice corrosion breakdown potential which sustained the increase of anodic current density. The occurrence of the hysteresis loop is related to the presence of aggressive solution formed inside the occluded area which maintain when the potential was reversed. Therefore, it was clear that the increase in the concentration significantly decreased the breakdown (pitting) potential and protection potential values. The corrosion parameters are given in Table (3).

As is clear from the table, corrosion potential E_{corr} decreased and corrosion current I_{corr} , increased with increasing the sodium chloride concentrations for both two types of electrodes. The pitting potential, E_{pit} , was invariably more positive than the protective potential, E_p .

Table (3): The corrosion parameters of electrodes I and II in different % of NaCl solutions.

Alloy type	NaCl %	E_{corr} . V	E_p V	E_{pit} . V	$I_{\text{corr}} \times 10^{-7}$ A/cm ²	$I_p \times 10^{-6}$ A/cm ²	$I_{\text{pit}} \times 10^{-4}$ A/cm ²
(I)	0.5	-0.150	0.347	1.240	2.91	6.73	0.82
	1.5	-0.192	-0.064	1.104	3.36	2.07	2.14
	3.5	-0.231	-0.145	0.456	4.16	2.56	4.77
	5.5	-0.426	-0.338	0.241	5.94	2.66	5.29
(II)	0.5	-0.141	0.053	0.499	1.82	2.15	0.14
	1.5	-0.178	-0.067	0.455	1.92	2.24	0.14
	3.5	-0.259	-0.163	0.227	2.45	2.88	0.16
	5.5	-0.362	-0.259	0.138	2.82	2.88	0.17

Hysteresis loop is observed during the reverse anodic scan which indicates the possibility of pitting. The pitting on the passive surface has been explained by a competitive adsorption mechanism in which chloride ions moves to the metal/oxide film interface at the metal surface. At a particular chloride concentration, a pitting potential, E_{pit} , develops which is sufficient to displace oxygen from the protective oxide layer⁽¹⁹⁾.

The relationship between pitting potential (E_{pit}), or protection potential (E_p) and the logarithm of chloride ion concentration at 25°C, for stainless steel electrodes type (I) and (II) is shown in figure(7). This figure revealed that both E_{pit} and E_p were linearly decreased with increase of the logarithm of chloride concentration at 25°C. The linear dependence of both E_{pit} and E_p on $\log [\text{Cl}^-]$ can be represented as:

$$E = \alpha - \beta \log [\text{Cl}^-]$$

Where; α and β are constants, dependent on the alloy composition and environment. The values obtained for constant β are -1.0066 and -0.6144; -0.3601 and -0.2887 mV/decade for variation of E_{pit} and E_p for electrodes type (I) and (II) respectively. The line of E_p versus $\log[\text{Cl}^-]$ is displaced, in the negative direction, from that for E_{pit} by 1.241 and 0.498V at low concentration for electrodes type I and II, respectively, and this value decreased to 0.428 and 0.138V at high concentration for two electrodes. This indicates that the initiated pitting corrosion on stainless steel can continue to grow when the potential was reduced less than those values. It has been reported that β values for different steels are dependent on the steel type and aggressiveness of the environment^(20, 21).

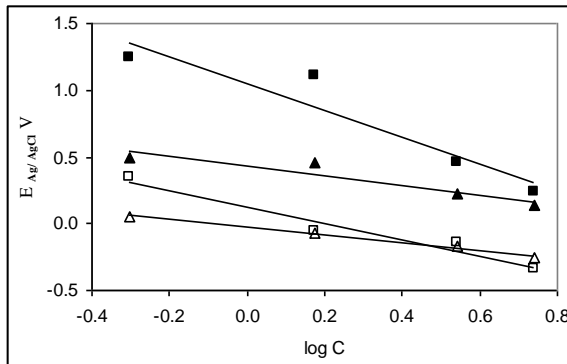


Figure (7): Effect of chloride ion concentration on E_p and E_{pit} For electrode type (I) and (II).

□ E_p (I) ■ E_{pit} (I) △ E_p (II) ▲ E_{pit} (II)

Spectroscopic analysis of pit on electrodes after 1 hr. experiment in NaCl solution, illustrates that, in 3.5% NaCl solution, an aggressive pitting attack with larger number of pits was observed on the surface of electrode type (I) (Figure 8, A). While electrode type (II) shows small pits which gathered to form large pit (Figure 8, B)

It was demonstrated that, in the case of austenitic stainless steel in NaCl solution, covered pits are formed which have a very small orifice in the covering layer, often not visible to the naked eye. Since such layers are rather thick, it seems likely that they are composed of the original passive film together with stable corrosion products deposited on the surface⁽²²⁾.

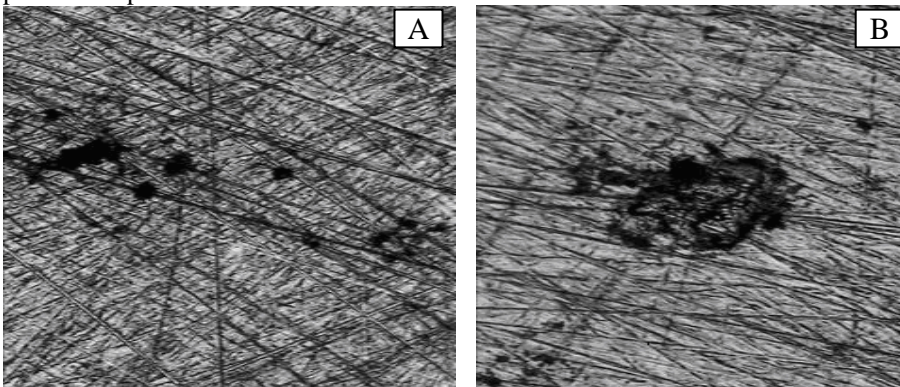


Figure (8): Spectroscopic analysis of pit on electrodes after 1 hr. experiment in 3.5% NaCl solution, (A) electrode I and (B) electrode II.

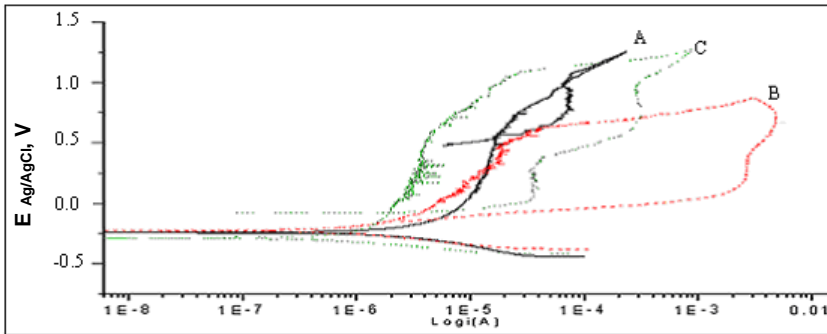
The oxide film has been improved by increasing nickel content in stainless steel electrode (II) because of its ability to stabilize the phase⁽²³⁾. Molybdenum may improve the oxide film by incorporation (probably as molybdates) into the structure of the oxide film^(24, 25). This may either change the electronic properties for instance by reversing the ion selectivity⁽²⁶⁻²⁹⁾ of the film making it more difficult for chloride ions to migrate through it, or take part in enhancing the oxide film by increasing the thickness⁽³⁰⁾. The possibility of any of these occurring is still being debated since the existence of molybdenum in the oxide film is doubtful⁽³¹⁻³³⁾.

The probability of stable pitting is dependent on the probability of activating sites capable of metastable pit growth and the probability of these metastable pits attaining stability. From the results obtained from figures (5-8) and Table (3), both these probabilities are higher in stainless steel electrode type (I) compared with type (II) and can be said to be responsible for its susceptibilities to pitting.

Figures (9, 10) represent the PCAP curves of stainless steel electrodes type (I) and (II) in 3.5% sodium chloride solution at different scan rate ranging from 0.5 to 2 mV/s.. The results show that increasing of scan rate leads to the increase of general corrosion on two stainless steels. A linear relationship is obtained between the anodic current peak (I_a) and the square root of the scan rate ($V^{0.5}$), Figure (11), the lines are passing near the zero value for (I_a) and scan rate. This indicates that the anodic current peaks are due to the dissolution of stainless steel to form the passive oxide layer and the dissolution process is controlled by the diffusion of the different anions, chloride, hydroxide and O^{2-} from the bulk of the solution to the electrolyte/stainless steel interface. This is, in principle, consistent with the participation of a diffusion process in the anodic reactions⁽³⁴⁾.

The corrosion parameters of stainless steel electrodes type (I) and (II) in 3.5% sodium chloride solution at different scan rates; 0.5, 1 and 2mV/sec. are given in Table (4). As can be seen from the table, corrosion potential, E_{corr} , protection potential, E_p , and pitting potential, $E_{pit.}$, values increases with increasing scan rate for two electrodes. This indicates that the increase of scan rate increase the breakdown, dissolution of passive film formed on the surface and consequently increases the localized pitting corrosion.

The higher scanning rate gives rise to a higher active anodic dissolution peak, which is shifted toward more noble potentials. As expected, the faster scan, the higher the positive current and nobler pitting potential. Good reproducibility was obtained with scan rate 1mV/sec.



Figure(9):Cyclic anodic polarization curves of electrode type (I) in 3.5% NaCl solutions with scan rate of: (A) 2mV/s (B) 1mV/s (C) 0.5mV/s.

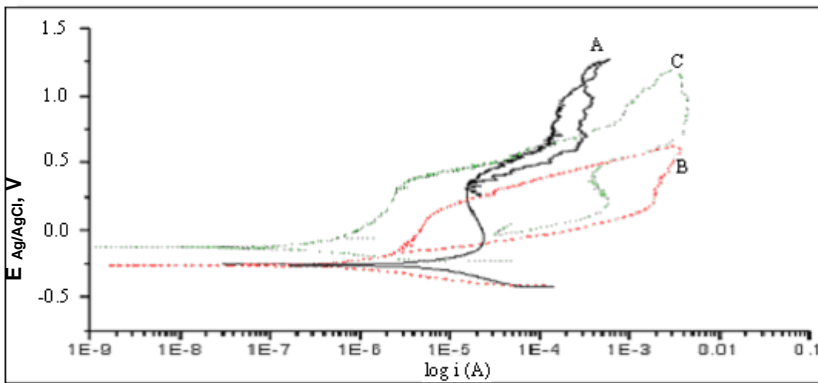


Figure (10): Cyclic anodic polarization curves of electrode type (II) in 3.5% NaCl solutions with scan rate of: (A) 2mV/s (B) 1mV/s (C) 0.5mV/s.

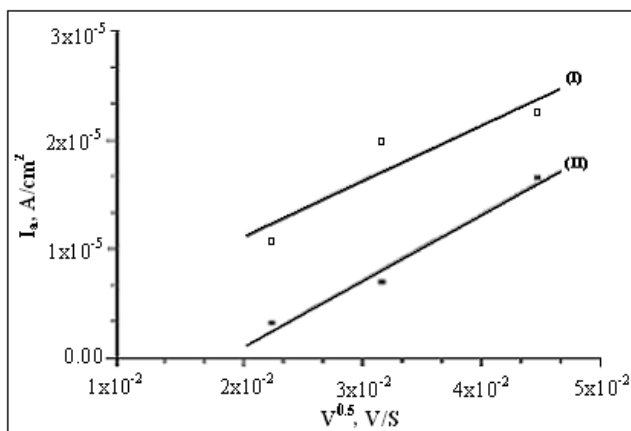


Figure (11): Anodic current peaks as a function of square root of scan rate in 3.5% NaCl solution for electrodes type (I) and (II)

Table (4): Corrosion parameters of electrode I and II in 3.5% NaCl, solutions with different scanning rates S_R .

	S_R mV/S	$E_{corr.}$ V	E_p V	E_{pit} V	$I_{corr.}$ A/cm ²	I_p A/cm ²	I_{pit} A/cm ²
(I)	0.5	-0.291	-.0179	0.235	4.21 E-7	1.95E-6	2.43E-5
	1.0	-0.231	-0.145	0.456	4.16 E-7	2.56E-6	4.77E-4
	2.0	-0.221	0.537	1.120	2.15 E-7	1.57E-5	1.06E-4
(II)	0.5	-0.281	-0.252	0.201	1.08 E-6	5.58E-7	4.69E-6
	1.0	-0.259	-0.163	0.227	2.45 E-7	2.88E-6	1.56E-5
	2.0	-0.258	0.328	1.050	19.9 E-7	1.57E-5	2.90E-4

C) *Effect of some additives to 3.5 % NaCl solution on the potentiodynamic cyclic anodic polarization of stainless steel electrodes.*

i- Effect of sodium thiosulphate additions:

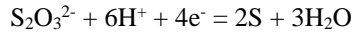
Figures (12, 13) show the PCAP curves of stainless steel electrodes type (I) and (II) in 3.5% sodium chloride solution with and without additions of different concentrations of sodium thiosulphate, ranging from 50 to 200 ppm., using scan rate 1mV/sec. at 25⁰C.

It is clear that, corrosion started in the form of pits, and proceeds as pitting corrosion on the free surface. Thiosulphate which have a slow diffusion rate increased the hysteresis loop and thus, increased the possible potential range of pits to grow. The ability of thiosulphate pits to grow seems to be merely a function of low repassivation potential rather than a function of low pitting potential⁽¹⁹⁾. At the potential where a rapid increase in current density occurred, a black corrosion product was found to precipitate on the specimen surface. However, as the potential was higher than 0.15V, the corrosion product disappeared. The results showed that the current density decreased drastically at the early stage when the potential was polarized at -0.2V.

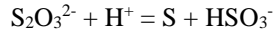
The decreases in current density were associated with the formation of passive film. Several current density peaks were found in the steady state region. These peaks are believed to be associated with the formation of meta-stable or unstable pits formed on the surface, which repassivated rapidly.

From the results of Table (5), it is found that there is no significant change in the corrosion potential values after the thiosulphate addition to NaCl solution, while protection potential, E_p , and pitting potential, E_{pit} , values decrease.

It is believed that thiosulphate ion reduced to $S_{(ads.)}$ and $H_2S_{(aq.)}$ on the surface and subsequently reacted with the dissociated Ni^{2+} to precipitate NiS. The sequence of reactions is explained as following, at first, $S_2O_3^{2-}$ was reduced to form S by the following reaction⁽³⁵⁾:



This contributes to the significant increase in the anodic current density. $\text{S}_2\text{O}_3^{2-}$ might also undergo disproportionation reaction to form H_2S and HSO_3^- .



Sulphur was further reduced and incorporated with H^+ to form H_2S which eventually reacted with the dissolved Ni^{2+} to precipitate NiS according to the following reactions⁽³⁶⁾:

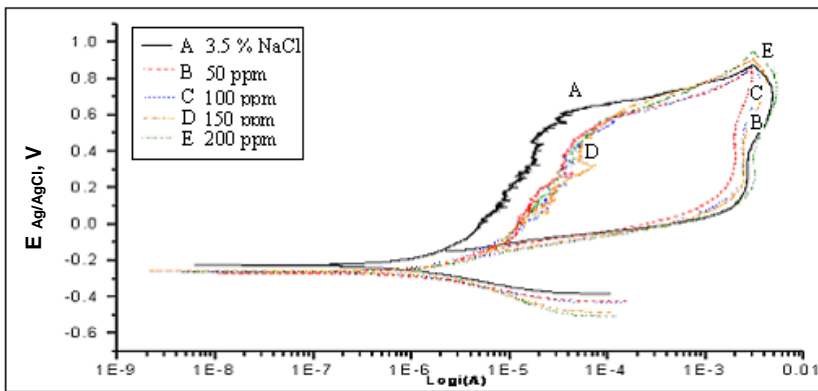
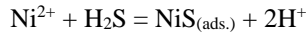
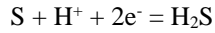


Figure (12): Cyclic anodic polarization curves of electrode type (I) in 3.5% NaCl solutions with (50-200ppm) $\text{Na}_2\text{S}_2\text{O}_3$ solutions.

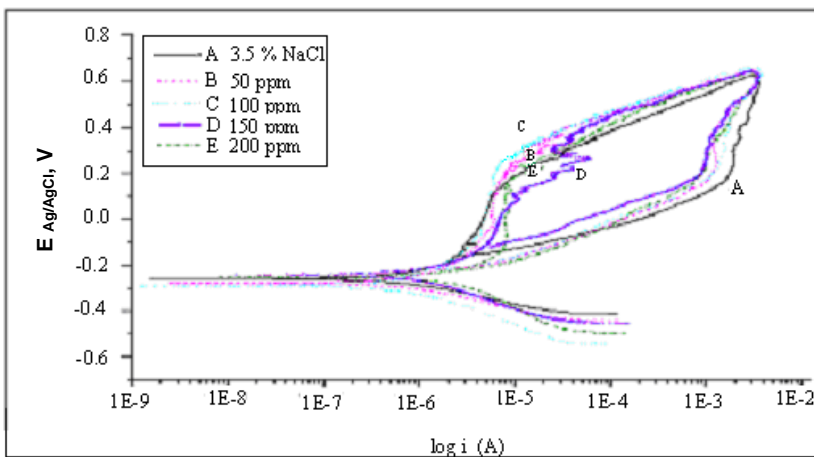
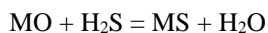


Figure (13): Cyclic anodic polarization curves of electrode type (II) in 3.5% NaCl solutions with (50-200ppm) $\text{Na}_2\text{S}_2\text{O}_3$ solutions.

It was also possible that the pre-existing metal oxide MO reacted with H₂S to form sulfide in accordance with the following reaction:



At potentials greater than 0.15V, the transformation of NiS to form Ni(OH)₂ is occurred.

Furthermore, in sodium chloride solution, the addition of sodium thiosulphate, enhanced pitting corrosion as compared with that found in pure sodium chloride solution^(37, 38). Although thiosulphate anions alone have not been found aggressive enough to cause damage to stainless steel, they have been shown to act in synergy with other common ions, such as chloride or sulphate to cause severe localized corrosion⁽³⁹⁾. Whether the synergistic effect of Cl⁻ and S₂O₃²⁻ still exists on pitting corrosion of a more pitting resistant high Cr austenitic stainless.

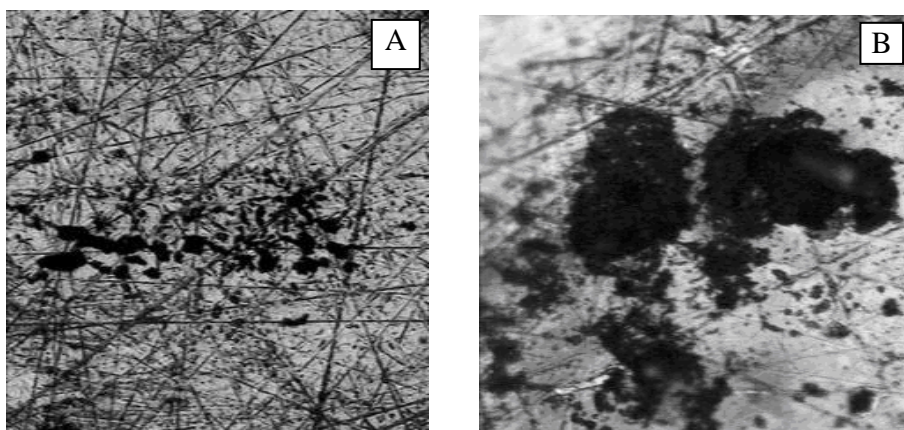
It is also found that there is a limited range of S₂O₃²⁻ ion concentration around 0.1M Na₂S₂O₃ at which the pitting potential of stainless steel is significantly lower than that recorded in pure chloride solution, while lower and higher concentrations of thiosulphate added to chloride have the same effect on pitting potential, E_{pit.}, which interpreted on the basis that an insufficient sulphur layer is formed at low concentration of S₂O₃²⁻ while the small effect of high concentration may be due to the retardation of the pit propagation process because of the preferential electromigration of S₂O₃²⁻ in the pit⁽¹⁹⁾.

Therefore, the effect of thiosulphate on localized corrosion has been explained in two different ways: 1- thiosulphate is reduced to elementary sulphur S⁰, which adsorbed on bare metallic surface preventing passivation, or 2- thiosulphate is reduced to hydrogen sulfide which catalyses the anodic dissolution of stainless steel.

Surface morphology illustrated that in the presence of the chloride-thiosulphate mixture, stronger pitting attack is observed and the pit is greater than that obtained in pure chloride this attributed to the synergistic effect of thiosulphate with chloride causing pitting corrosion. On the other hand, the pits formed in chloride-thiosulphate, are deeper, larger and more elongated than those formed in pure chloride as shown in Figure (14). It is clear from the figure that the pits formed are quite shallow, and sometimes two pits are joined together to form more extensive local attack and they are visible to the naked eye.

Table (5): The corrosion parameters of electrode I and II in 3.5% NaCl containing (50-200 ppm.) sodium thiosulphate solutions.

Alloy type	Wt. of S ₂ O ₃ ²⁻ ppm.	E _{corr.} V	E _p V	E _{pit.} V
(I)	0	-0.231	-0.145	0.456
	50	-0.268	-0.145	0.575
	100	-0.263	-0.190	0.564
	150	-0.263	-0.196	0.545
	200	-0.266	-0.205	0.535
(II)	0	-0.259	-0.163	0.227
	50	-0.278	-0.210	0.217
	100	-0.290	-0.219	0.212
	150	-0.246	-0.120	0.201
	200	-0.255	-0.220	0.181

**Figure (14): Spectroscopic analysis of pit on electrodes after 1 hr. Experiment in 3.5% NaCl + Na₂S₂O₃ solution, (A) electrode I and (B) electrode II.**

ii- Study of the efficiency of 3-amino-1, 2, 4-triazole (AT) as inhibitive species towards pitting corrosion of stainless steel:

Figures (15,16) represent the PCAP measurements for stainless steel electrodes type (I) and (II) in 3.5% sodium chloride solution with and without additions of different concentrations of 3-amino-1,2,4-triazole(AT) using scanning rate 1mV/sec. in the potential range from -600 to 1400 mVAg/AgCl at 25°C. The corrosion parameters of stainless steel electrodes and inhibition efficiency, I.E% are given in Table (6).

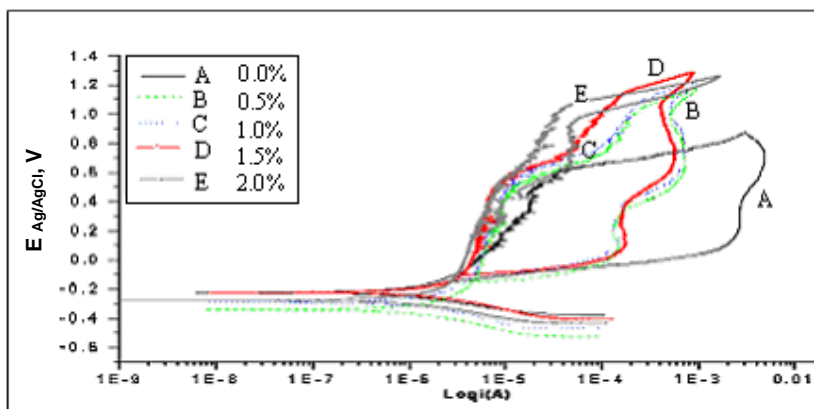


Figure (15): Cyclic anodic polarization curves of electrode type (I) in 3.5% NaCl solutions with 0.5-2%AT inhibitor.

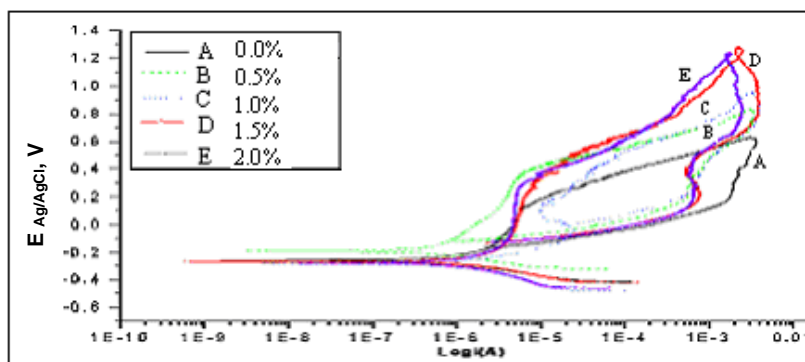
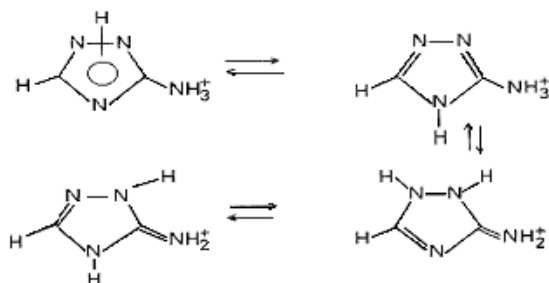


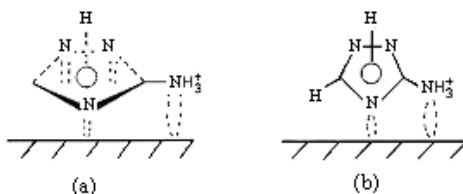
Figure (16): Cyclic anodic polarization curves of electrode type (II) in 3.5% NaCl solutions with 0.5-2%AT inhibitor.

From the experimental results obtained, it is found that at good conditions, the hysteresis loop observed during the reverse anodic scan which indicates the possibility of pitting corrosion is diminished as the concentration of aminotriazole added to 3.5% NaCl is increased. It is clear that the cathodic reaction (hydrogen evolution) is inhibited and inhibition increases as the inhibitor concentration increases. Values of protection potential, pitting potential and inhibition efficiency are increased as the concentration of aminotriazole (AT) added to 3.5% NaCl increased for type I and II; while corrosion potential and corrosion current decreased for both electrodes. The diminishing of hysteresis loop and increasing of the corrosion parameters indicate that AT has a much more significant effect. This implies that the corrosion inhibition is due to the presence of amino group in the molecular structure.

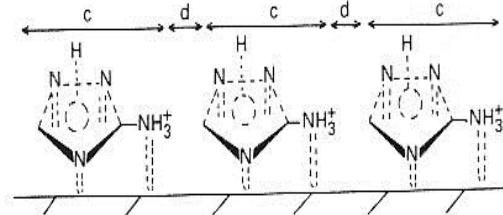
The AT inhibitory action may be attributed to the formation of a thick and relatively compact film at the stainless steel surface. An attempt was made to correlate AT electrochemical behavior and its molecular structure. Nevertheless, no N-substituted 1, 2, 4-triazole type organic compound present a planar structure and tend to exist in different tautomeric forms resulting from the non-localized hydrogen of the triazole cycle^(40, 41). In this case the four tautomeric forms are:



The adsorption of the protonated form of AT is favored by the attractive interaction between the Cl^- anions adsorbed and the cations of inhibitor. When the different models of AT adsorption are considered, the following models are possible:

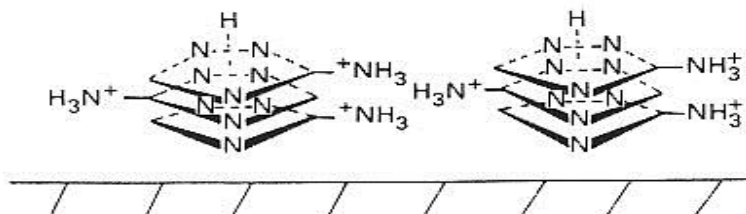


The flat model (a) is stable and preferred since the covered fraction of surface is high, even at low concentrations, and thus explains the cathodic effect of the AT. This adsorption model is favored by establishing “donor-acceptor” links between the empty d-orbital of iron and the pairs of free electrons on the nitrogen atoms and by the electrostatic interactions between NH_3^+ and the adsorbed Cl^- anions on the surface. The increase in surface coverage with increase in concentration of AT may be illustrated by the following representation⁽⁴²⁾:



In this case two pictures of the surface may be investigated; i) a fraction of the surface is covered by adsorbed AT molecules with cathodic and anodic sites (represented by area c), ii) the non-covered surface (represented by area d) is in direct contact with the electrolyte. On this fraction of electrode surface the hydrogen reaction occurs, confirming the non-modification of their mechanism upon the addition of AT.

The adsorption of AT, which gives rise to excellent corrosion inhibition must necessarily be followed by molecular stacking on the surface. This lead to the establishment of a stable and relatively thick 3D inhibition layer as follows:



Therefore, it is concluded that the AT acts as cathodic inhibitor and the cathodic corrosion inhibition of AT is interpreted by partial blocking of the electrode surface due to adsorption of protonated species according to the Langmuir isotherm on the surface. Hydrogen reduction occurs on the electrode surface which is not covered by the AT film.

Table (6): The corrosion parameters of electrode I and II in 3.5 % NaCl containing different % of AT inhibitor.

AT %	$E_{corr.}$ V	E_p V	$E_{pit.}$ V	$I_{corr.} \times 10^{-7}$ A/cm ²	I_p A/cm ²	$I_{pit.} \times 10^{-5}$ A/cm ²	IE%
0.0	-0.231	-0.145	0.456	4.16	2.56E-6	47.70	--
0.5	-0.245	-0.145	0.741	1.48	4.82E-6	10.70	64.42
(I) 1.0	-0.273	-0.109	0.768	1.39	4.65E-6	7.88	66.59
1.5	-0.284	-0.094	0.788	1.08	3.26E-6	5.31	74.04
2.0	-0.291	0.141	1.040	0.92	3.14E-6	3.98	77.79
0.0	-0.259	-0.163	0.227	2.45	2.88E-6	1.56	--
0.5	-0.192	-0.119	0.425	1.01	8.49E-7	1.05	58.78
(II) 1.0	-0.257	-0.118	0.444	0.98	2.02E-5	1.08	59.88
1.5	-0.263	-0.111	0.512	0.76	3.49E-6	1.61	68.90
2.0	-0.286	-0.114	0.545	0.66	3.24E-6	1.02	72.98

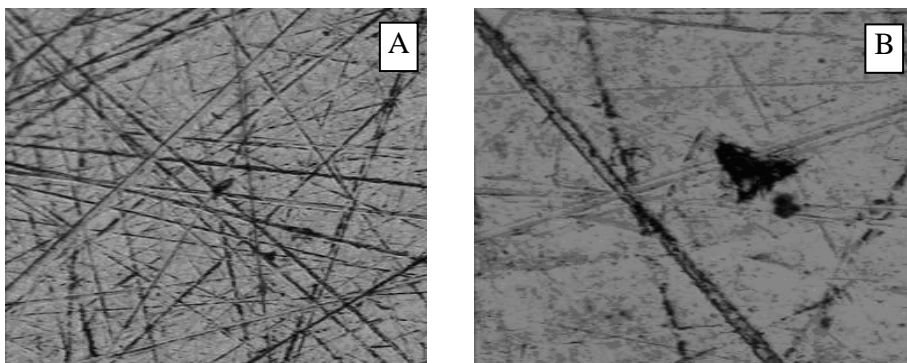


Figure17: Spectroscopic analysis of pit on electrodes after 1 hr. experiment in 3.5% NaCl +2% AT solution A) electrode I B) electrode II

iii- Study of the efficiency of 4-amino-5-mercapto-1,2,4-triazole, (AMT) as inhibitive species towards pitting corrosion of stainless steel:

Figures (18and19) show the effect of different concentrations of 4-amino-5-mercapto-1,2,4-triazole (AMT) on the electrochemical behavior of stainless steel electrodes in 3.5% sodium chloride solution, using scan rate 1mV/sec. at 25°C.

Increasing concentration of AMT increases protection potential, pitting potential and inhibition efficiency values for the two electrodes, indicating the pitting corrosion inhibition (Table 7). AMT decreased corrosion current significantly in all the concentrations added. Both the anodic and cathodic current densities are decreased indicating that AMT suppressed both anodic and cathodic reactions. This suggested a mixed-type control and AMT mainly acts as a mixed type inhibitor in 3.5% NaCl.

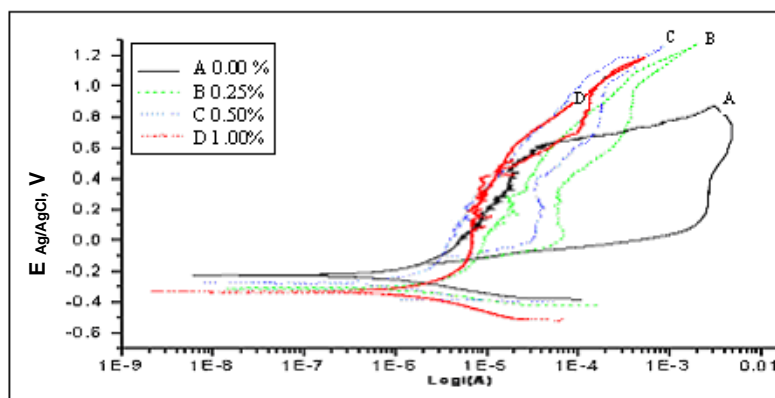


Figure (18): Cyclic anodic polarization curves of electrode type (I) in 3.5% NaCl solutions with 3.5-1%AMT inhibitor.

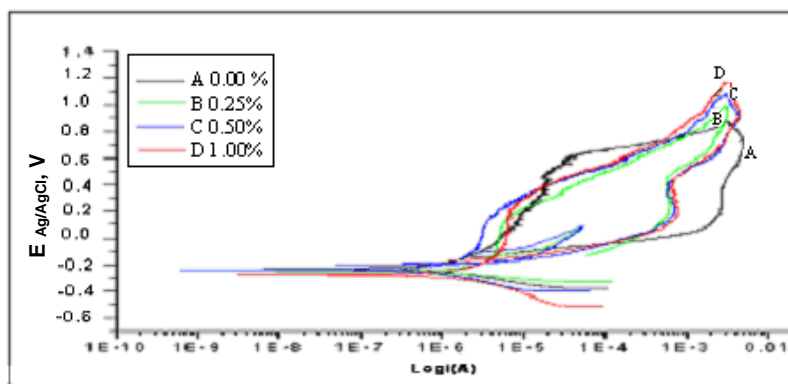
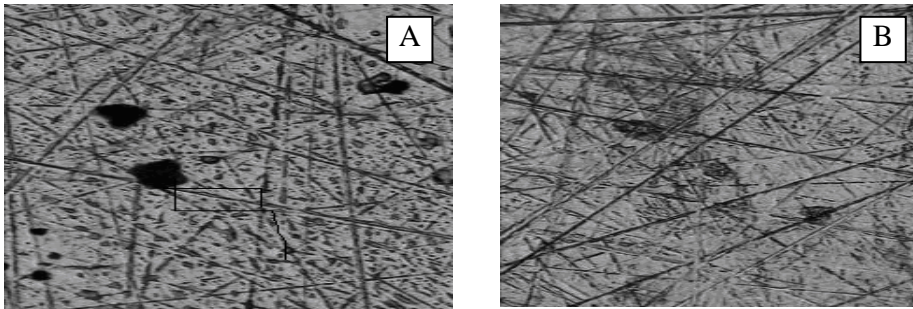


Figure (19): Cyclic anodic polarization curves of electrode type (II) in 3.5% NaCl solutions with 3.5-1% AMT inhibitor.

Table (7): Corrosion parameters of electrode I and II in 3.5 % NaCl containing different % of AMT inhibitor.

	AMT %	$E_{corr.}$ V	E_p V	E_{pit} V	$I_{corr.} \times 10^{-7}$ A/cm ²	$I_p \times 10^{-6}$ A/cm ²	$I_{pit} \times 10^{-5}$ A/cm ²	I.E%
(I)	0.00	-0.231	-0.145	0.456	4.16	2.56	47.69	--
	0.25	-0.309	-0.110	1.070	2.69	6.50	3.22	35.36
	0.50	-0.284	-0.104	1.180	1.37	6.93	2.63	67.07
	1.00	-0.338	0.451	1.190	1.21	9.40	4.85	70.91
(II)	0.00	-0.259	-0.163	0.227	2.45	2.88	1.56	--
	0.25	-0.255	-0.187	0.423	1.01	3.07	3.39	58.78
	0.50	-0.236	-0.181	0.496	0.97	2.21	2.55	60.20
	1.00	-0.276	0.571	0.681	0.92	2.95	8.11	62.45

Figure 20 represents the spectroscopic analysis of pit on the two electrodes after 1 hr. experiment in 3.5% NaCl with 1% AMT solution. Inhibition of corrosion of stainless steel in NaCl solution by the amino-mercapto-triazole can be explained on the basis of adsorption on the metal surface. This can occur directly on the basis of donor-acceptor interaction between the lone pairs of the heteroatom and the extensively delocalized π -electrons of the mercapto-triazole molecule and the vacant d-orbital of iron surface atoms⁽⁴³⁾. Moreover, the presence of mercapto compound in the organic structure makes the formation of $d\pi-d\pi$ bond resulting from overlap of 3d electrons from Fe atom to the 3d vacant orbital of the sulphur atom possible, which enhances the adsorption of the compounds on the metal surface. The compound inhibits the pitting corrosion by controlling both anodic and cathodic reactions. AMT is able to adsorb on anodic sites through N and S atoms, heterocyclic and aromatic rings which are electron donating groups. The adsorption of this compound on anodic sites may decrease anodic dissolution of stainless steel⁽⁴⁴⁾.



Figure(20): Spectroscopic analysis of pit on electrodes after 1 hr. experiment in 3.5% NaCl +1% AMT solution A) Electrode I B) Electrode II

Comparison of the curves plotted for stainless steel in 3.5% NaCl solution with and without 1.0% AT and AMT inhibitor species show that AT and AMT shifted the pitting and protection potentials to the noble direction and diminished the hysteresis loop of the revers scan in the PCAP curves (Figure 21, 22).

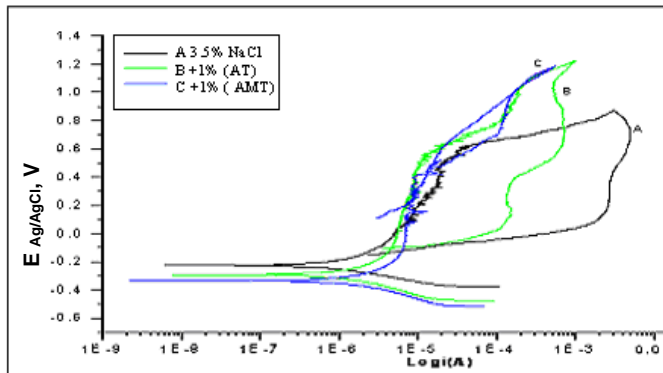


Figure (21): Cyclic anodic polarization curves of electrode type (I) in 3.5% NaCl solutions with 1% AT and AMT inhibitors.

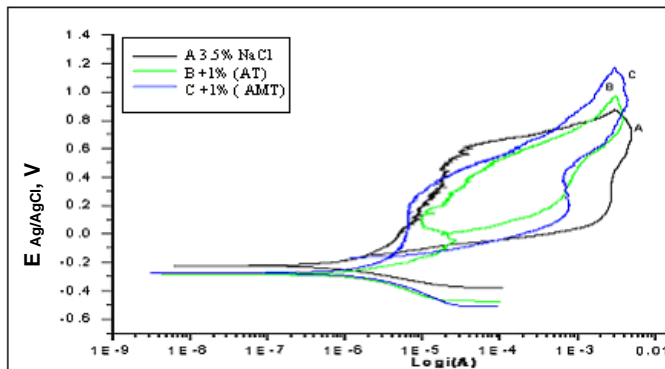


Figure (22): Cyclic anodic polarization curves of electrode type (II) in 3.5% NaCl solutions with 1% AT and AMT inhibitors.

From Tables (6,7), it is clear that the inhibition efficiency calculated is decreased in the order $AMT > AT$. The lesser value of inhibition efficiency for AT as compared to AMT can be attributed to the lower electron densities around the chemisorptions center. It is also found that the pitting potential and protection potential shifted to more anodic values. From the experimental results, it is concluded that the inhibitive properties of such triazole derivatives depend mainly on the electron densities around the adsorption center and the molecular size. So, the introduction of strong electron donating groups in the triazole heterocycle or the replacement of hydrogen atom on the mercapto substituent by alkyl or aryl groups may result in more corrosion inhibitions.

The variation of inhibition effect of AT and AMT in 3.5% NaCl solution for stainless steel electrode type (I) and (II) may be due to the change in the composition of two electrodes. The inhibition efficiency values indicate that electrode type (I) is more inhibited and influence by the effect of both AT and AMT while electrode type (II) still more activated in chloride solution with triazoles additions. The increase of the Ni percent in the electrode type (II) may be increase the probability of dissolution of the complex layer formed between the stainless steel surface and inhibitor.

The micrograph reveals that AT and AMT are adsorbed on the surface of the two electrodes forming a good protective film present on the stainless steel surface. This confirms the highest inhibition efficiency of the two inhibitors.

As a result, AT and AMT can be used as inhibitors for stainless steel in sodium chloride solution to reduce the aggressiveness of the chloride medium in which the additive inhibitors improve the surface conditions of two stainless steel electrodes.

Also the visual investigation (by using normal camera) of pits on electrodes type (I) and (II) after the corrosion testes in previous all test solutions are shown in figure (23).









Electrode Type	3.5% NaCl	3.5% NaCl + 200 ppm. $Na_2S_2O_3$	3.5% NaCl +2%AT	3.5% NaCl +2%AMT
(I)				
(II)				

Figure (23): Visual investigation of pit on electrode type (I) and (II) after 1hr experiment.

Table (8): Metallographic examination of electrodes I and II

Medium	3.5%NaCl		3.5%NaCl+ 200ppm.Na ₂ S ₂ O ₃		3.5%NaCl+ 2%AT		3.5%NaCl+ 1%AMT	
	(I)	(II)	(I)	(II)	(I)	(II)	(I)	(II)
Electrode type	(I)	(II)	(I)	(II)	(I)	(II)	(I)	(II)
Number of pits/cm ²	15	7	20	18	2	1	1	1
Maximum pit depth in μm	6	4	12	11	2	1	2	1

data in Table 8 confirm that the number of pits and maximum pit depth in case of electrode (I) is greater than that in electrode type (II) which is in agreement with the results obtained by using potentiodynamic cyclic anodic polarization.

References

1. Anon; Advanced materials and processes, 154 (4) pp. 63, (1998).
2. W.F. Smith; Structure and properties of engineering alloys, McGraw-Hill, Inc., second edition, Chapter 7, (1993).
3. B.C. Wang and J.h. Zhu; Ultrasonics Sonochemistry, 15(3) pp.239, (2008).
4. M.Z.A. Rafiquee, N. Saxena, S. Khan and M.A. Quraishi; Materials Chemistry and Physics, 107(2-3), pp.528, (2008).
5. H. H. Hassan; Electrochim. Acta, 53(4) pp.1722, (2007).
6. V. R. Saliyan and A. V. Adhikari; Corros. Sci., 50 (1) pp. 55, (2008).
7. K. Tebbji, N. Faska, A. Tounsi, H. Oudda, M. Benkaddour and B. Hammouti; Mater. Chem. and Phy. 106 (2-3) pp. 260, (2007).
8. A.Y. El-Etre; Journal of Colloid and Interface Science 314 (2) pp. 578, (2007).
9. M. Benabdellah, R. Touzani, A. Aouniti, A. Dafali, S. El Kadiri, B. Hammouti and M. Benkaddour; Mater. Chem. and Phy., 105 (2-3) pp. 373, (2007).
10. K. Tebbji, A. Aouniti, M. Benkaddour, H. Oudda, I. Bouabdallah, B. Hammouti and A. Ramdani; Progress in Organic Coatings 54 (3) pp. 170, (2005).
11. K. Tebbji, B. Hammouti, H. Oudda, A. Ramdani and M. Benkaddour; Applied Surface Science, 252(5) pp. 1378, (2005).
12. L.F. Li, P. Caenen, M. Daerden, D. Vaes, G. Meers, C. Dhondt and J. P. Celis; Corros. Sci. 47 (5) pp. 1307, (2005).
13. L.F. Li, M. Daerden, P. Caenen and J.P. Celis; Passivation of Metals and Semiconductors, and Properties of Thin Oxide Layers, pp. 579, (2006).
14. B. E. Wilde and E. Williams; Electrochemi. Acta, 16 pp. 1971, (1971).

15. M. Pourbaix; Atlas of Electrochemical Equilibria in Aqueous Solutions, 2nd ed., National Association of Corrosion Engineering. Houston, TX, USA (1974).
16. S. Godn, Eklund; Journal of the Electrochemical Society, 121, pp. 467, (1974).
17. E. A. Abd El Meguid and A.A. Abd El Latif; Corros. Sci. 46 pp. 2431, (2004).
18. T. Rogne, J. M. Drugli and S. Valen; Corros. 48 pp. 864, (1992).
19. E. A. Abd El Meguid and N. A. Mahmoud; 17th Annual Conference Corrosion Problems in Industry, 1-3, (1998).
20. E. A. Abd El Meguid, N. A. Mahmoud and V. K.Gouda; J. Br. Corros. 33 pp. 42, (1998).
21. E. A. Abd El Meguid; Corros. 53 pp. 623, (1997).
22. Z. Smialowska, Szklarska; Localized Corrosion, NACE, Houston, Tex, 312, (1974).
23. A.A. Hermas, K. Ogura, S. Tagaki, and T. Adachi; Corrosion, 51 pp. 3, (1995).
24. C.R. Clayton, and Y. C. Lu; J. Electrochem. Soc., 133, pp. 2465, (1986).
25. I. Olefjord and B. Elfstorm; Corrosion, 38, pp. 46, (1982).
26. J. Baszkiewicz, M. Kaminski, A. Podgorki, J. Jagielski, and G. Gawlik; Corros. Sci., 33, pp. 815, (1992).
27. M. Sakashita and N. sato; Corrosion, 35, pp. 351, (1979).
28. Y. C. Lu, C. R. Clayton and A. R. Brookes; Corros. Sci., 29, pp. 863, (1989).
29. B. D. Craig, Fundamental Aspects of Corrosion Films in Corrosion Science, Plenum Press, New York, USA, (1991).
30. K. Sugimoto and Y. Sawada; Corros. Sci., 17, pp. 425, (1977).
31. J. R. Cahoon and R. Bandy; Corros., 38, pp. 299, (1982).
32. A. E. Yamiv, J. B. Lumsden and R. W. Staehle; J. Electrochem. Soc., 124, pp. 490, (1977).
33. J. R. Galvele, J. B. Lumsden and R. W. Staehle; J. Electrochem. Soc., 125, pp. 1204, (1978).
34. S. A. M. Refaey, F. Taha and A. M. Abd El Malak; Appl. Sur. Sci., 242, pp. 114, (2005).
35. R. J. Biernat and R. G. Robins; Electrochem. Acta, 14, pp. 809, (1969).
36. A. Okuwaki, O. Kanme and Okabe; Metallurgical Transaction, 15 (12), pp. 609, (1984).
37. J. O. Park, M. Verhoff and R. Alkire; Electrochem. Acta, 42, pp. 3281, (1997).
38. R. Roberge, Corros., 44, pp. 274, (1988).
39. P. R. Roberge, S. Wang and R. Roberge; Corros., 52, pp. 733, (1996).

40. M. Saidi Idrissi, P. Lannane and C. Garrigou Lagrange; *J. Phy. Chem.*, 78, pp. 510, (1981).
41. S. Zaydoun, M. Saidi Idrissi and C. Garrigou Lagrange; *Spectrochem. Acta*, 44, pp. 1421, (1988).
42. S. Kertit, F. Chaouket, A. Srhiri and M. Keddami; *J. Appl. Electrochem.*, 24, pp. 1139, (1994).
43. S. Muralidharan, M. A. Quraishi and S. V. K. Lyer; *Corros. Sci.*, 37, pp. 1739, (1995).
44. B. Bonnelly, T. C. Downie, R. Grzekowiak, H. R. Hamburg and D. Short; *Corros. Sci.*, 18, pp. 109, (1978).